# PCCP



**PAPER** 

View Article Online



Cite this: Phys. Chem. Chem. Phys., 2024, 26, 15181

# A two-step quadrature-based variational calculation of ro-vibrational levels and wavefunctions of CO<sub>2</sub> using a bisector-x molecule-fixed frame†

Xiao-Gang Wang and Tucker Carrington Jr

In this paper, we propose a new two-step strategy for computing ro-vibrational energy levels and wavefunctions of a triatomic molecule and apply it to CO<sub>2</sub>. A two-step method [J. Tennyson and B. T. Sutcliffe, Mol. Phys., 1986, 58, 1067] uses a basis whose functions are products of K-dependent "vibrational" functions and symmetric top functions. K is the quantum number for the molecule-fixed zcomponent of the angular momentum. For a linear molecule, a two-step method is efficient because the Hamiltonian used to compute the basis functions includes the largest coupling term. The most important distinguishing feature of the two-step method we propose is that it uses an associated Legendre basis and quadrature rather than a K-dependent discrete variable representation. This reduces the cost of the calculation and simplifies the method. We have computed ro-vibrational energy levels with J up to 100 for  $CO_2$ , on an accurate available potential energy surface which is known as the AMES-2 PES and present a subset of those levels. We have converged most levels up to 20 000 cm<sup>-1</sup> to  $0.0001 \text{ cm}^{-1}$ .

Received 14th February 2024, Accepted 2nd April 2024

DOI: 10.1039/d4cp00655k

rsc.li/pccp

#### I. Introduction

Many variational methods have been proposed for computing solutions to the ro-vibrational Schröedinger equation for triatomic molecules<sup>1-11</sup> and all of the components of the method we propose in this paper are known, but they have not previously been combined in the way we suggest. Our method is quadrature-based and simple and efficient. We demonstrate its advantages by computing ro-vibrational energy levels of CO<sub>2</sub> up to 20 000 cm<sup>-1</sup> above the zero point energy.

The cornerstone of our approach is the two-step method of Tennyson and Sutcliffe.9 It shares many features with other contracted basis methods. 2,12,13 In a two-step calculation, one first computes eigenfunctions,  $|v^{(K)}\rangle$ , of a Hamiltonian, extracted from the full Hamiltonian, that depends on vibrational coordinates, but is also labelled by K, the quantum number associated with the molecule-fixed z component of the angular momentum. In the second step of the calculation, one computes eigenvalues and eigenvectors of a matrix representing the full Hamiltonian, in a basis of products of  $|v^{(K)}\rangle$  and symmetric top eigenfunctions | JKM \rangle. Instead of using the two-

Chemistry Department, Queen's University, Kingston, Ontario K7L 3N6, Canada. E-mail: xgwang.dalian@gmail.com, Tucker.Carrington@queensu.ca

step method, one could use a basis of products of J = 0eigenfunctions,  $|v^{(J=0)}\rangle$ , and  $|JKM\rangle$ . The most important disadvantage of this approach for linear molecules is that matrix elements off-diagonal in  $|v^{(J=0)}\rangle$  are large. In many two-step calculations, the number of  $|v^{(K)}\rangle$  is independent of K. When the goal is to compute all states below some threshold, we show that it is better to choose the number of  $|v^{(K)}\rangle$  functions using a cut-off energy (and therefore use fewer functions when K is larger). We also note that if K is larger than some maximum value, no  $|v^{(K)}\rangle$  are required. The required number of  $|v^{(K)}\rangle$ functions depends more sensitively on K, and decreases more quickly with K, for linear molecules, because for linear molecules  $\sin \theta$  in the term moved to the vibrational Hamiltonian is small where vibrational wavefunctions are large. We use Radau coordinates  $^{14,15}$  and a bisector-x molecule-fixed axis system. Both have been used before in two-step calculations.

The most important difference between our two-step method and the traditional two-step approach, as exemplified in the code DVR3D,5,6 is the primitive basis used to compute  $|v^{(K)}\rangle$ . For the bend coordinate, DVR3D uses a K-dependent discrete variable representation (DVR) basis 12,16,17 and we use an associated Legendre function (ALF) basis and a K-independent quadrature. Using an ALF basis obviates the need to transform matrix elements into a DVR and reduces the cost of the calculation. Using a DVR basis has the obvious advantage that the potential matrix is diagonal, however, it is straightforward and

<sup>†</sup> Electronic supplementary information (ESI) available. See DOI: https://doi.org/ 10.1039/d4cp00655k

inexpensive to evaluate matrix-vector products (and hence compute eigenvalues and eigenvectors) with a potential matrix in the ALF basis by evaluating sums sequentially.  $^{10,17,18}$  Another difference between our approach and DVR3D is that we compute  $|\nu^{(\mathcal{K})}\rangle$  with an iterative eigensolver, which makes it possible to use large primitive bases. It is also possible using successive contractions, as in DVR3D, to use a large primitive basis, but successive contractions means extra steps in the calculation. These differences are most important when J is large.

The new combination of ideas is tested by using it to compute many energy levels of CO2. CO2 is a popular test molecule because it is an important greenhouse gas and a significant component of the atmospheres of many planets in our solar system. 19,20 The spectrum of CO2 has been studied extensively. 21-23 A complete line list for CO<sub>2</sub> will be useful tool for studying environmental and physical conditions of planetary atmospheres. There are many theoretical calculations of rovibrational levels of CO2. The best and the most recent are those of Zak et al., 24 Huang et al., 25-27 and Yurchenko et al. 28 All of these papers report a CO2 line list. Zak et al. used DVR3D which is a numerically exact method. Yurchenko et al. used a TROVE method with some approximations. Huang et al. use their VTET code which is also numerically exact. They use a multi-step contraction that incorporates stretch-bend coupling in the final diagonalization which is sub-optimal for CO<sub>2</sub>, because stretch-bend coupling is important. It is better to contract together all the vibrational coordinates in the first step, but this is costly for larger molecules.

# II. Coordinates and kinetic energy operator

We use Radau coordinates<sup>14,15</sup> because they simplify the kinetic energy operator (KEO). We attach molecule-fixed axes to CO<sub>2</sub> by using the bisector-x embedding, in which the x-axis is antiparallel to the bisector vector  $R_2\vec{R}_1 + R_1\vec{R}_2$ . The z-axis is in the molecular plane with  $\vec{R}_1$  having a positive z component.  $\vec{R}_1$  and  $\vec{R}_2$  are the Radau vectors see Fig. 1. The bisector-x KEO was first

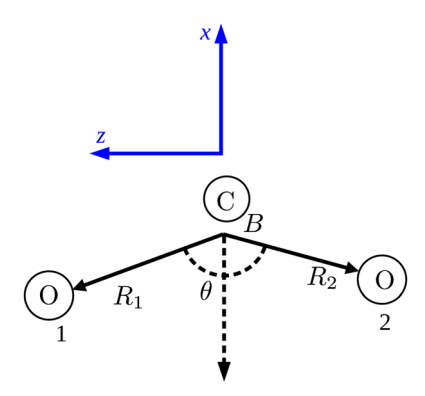


**Fig. 1** The Radau coordinates  $(R_1, R_2, \theta)$  and the bisector-x molecule-fixed frame (in blue). B is the canonical point. The dashed arrow is the bisector vector for  $\theta$ . The origin of the molecule-fixed frame is not at the center of mass of the molecule for clarity.

derived by Carter, Handy and Sutcliffe. <sup>29</sup> Our KEO is different from theirs because the direction of the *z*-axis is reversed, and our molecule-fixed angular momentum operators satisfy the anomalous commutation relation (see ref. 30). We choose the bisector-x embedding because it makes it easy to exploit the symmetry of  $CO_2$  and reduces the ro-vibrational coupling. The ro-vibrational KEO we use has two parts: a vibrational term  $T_v$  and a ro-vibrational term  $T_{vr}$ ,

$$T = T_{v} + T_{vr}.$$

$$T_{v} = -\frac{1}{2\mu_{R_{1}}} \frac{\partial^{2}}{\partial R_{1}^{2}} - \frac{1}{2\mu_{R_{2}}} \frac{\partial^{2}}{\partial R_{2}^{2}} - \left[B_{R_{1}}(R_{1}) + B_{R_{2}}(R_{2})\right]$$

$$\times \frac{1}{\sin \theta} \frac{\partial}{\partial \theta} \sin \theta \frac{\partial}{\partial \theta},$$

$$T_{vr} = \frac{1}{2} \left[B_{R_{1}}(R_{1}) + B_{R_{2}}(R_{2})\right] \left[\frac{1}{1 - \cos \theta} J_{x}^{2} + \frac{1}{2} J_{y}^{2} + \frac{1}{1 + \cos \theta} J_{z}^{2}\right]$$

$$+ \left[B_{R_{1}}(R_{1}) - B_{R_{2}}(R_{2})\right] \left[\frac{1}{2 \sin \theta} \{J_{x}, J_{z}\} + p_{\theta}^{H} J_{y}\right],$$

$$(2)$$

where

$$p_{\theta}^{H} = -i\left(\frac{\partial}{\partial \theta} + \frac{1}{2}\cot\theta\right) \tag{3}$$

is a Hermitian momentum operator and  $B_{R_i}(R_i) = 1/(2\mu_{R_i}R_i^2)$ .  $\mu_{R_i}$  are the masses of the atoms at the ends of the Radau vectors. The KEO is used with the volume element  $\sin\theta dR_1dR_2d\theta$   $\sin\beta d\alpha d\beta d\gamma$ .  $\alpha$ ,  $\beta$ ,  $\gamma$  are Euler angles. The ro-vibrational term can be re-written in terms of G matrix elements

$$T_{\text{vr}} = \frac{1}{2} \left[ G_{x,x} J_x^2 + G_{y,y} J_y^2 + G_{z,z} J_z^2 + G_{x,z} \{ J_x, J_z \} \right] + \frac{1}{2} \left( p_{\theta}^H G_{y,\theta} + G_{y,\theta} p_{\theta}^H \right) J_y,$$

$$(4)$$

where the G matrix elements are functions of the shape coordinates and, according to eqn (2), are

$$G_{x,x} = [B_{R_1}(R_1) + B_{R_2}(R_2)] \frac{1}{1 - \cos \theta}$$

$$G_{y,y} = \frac{1}{2} [B_{R_1}(R_1) + B_{R_2}(R_2)]$$

$$G_{z,z} = [B_{R_1}(R_1) + B_{R_2}(R_2)] \frac{1}{1 + \cos \theta}$$

$$G_{x,z} = [B_{R_1}(R_1) - B_{R_2}(R_2)] \frac{1}{\sin \theta}$$

$$G_{y,\theta} = [B_{R_1}(R_1) - B_{R_2}(R_2)].$$
(5)

When using Radau coordinates for a triatomic molecule it is also common to attach the molecular axis system so that the z axis is along a Radau vector. We call this a vector-z frame. Regardless of the embedding, some G matrix elements are singular at linear shapes. The vector-z frame has the advantage that basis functions can be chosen so that all KEO matrix

elements are finite. For CO<sub>2</sub>, the bisector-x embedding has two advantages over the vector-z frame: (i) it allows full exploitation of the permutation symmetry of the O atoms; (ii) the  $\Delta K = \pm 1$ and  $\Delta K = \pm 2$  matrix elements are small since at the equilibrium geometry, where the molecule is linear, the former are zero because  $G_{y,\theta} = G_{x,z} = 0$  and the latter are zero because  $G_{x,x} = G_{y,y}$ .

## III. Two-step variational calculation

We compute ro-vibrational energy levels and wavefunctions by using a two-step variational method. Each basis function is a product of a contracted vibrational function and a rotational function,

$$|v^{(K)}\rangle|JKM\rangle$$
. (6)

 $|v^{(K)}\rangle$  is an eigenfunction of a modified "vibrational" Hamiltonian

$$\tilde{H}_{v} = [\tilde{T}_{v} + V(R_{1}, R_{2}, \theta)], \tag{7}$$

$$\tilde{H}_{\mathbf{v}}|v^{(K)}\rangle = \mathcal{E}_{\mathbf{v}}^{(K)}|v^{(K)}\rangle.$$
 (8)

 $|JKM\rangle$  is a symmetric top eigenfunction (or Wigner function). In the basis of eqn (6),  $\tilde{H}_{v}$  is diagonal, the off-diagonal elements of  $\tilde{T}_{\rm vr}$  are small, and convergence with respect to the size of the basis is very fast. We retain the  $|v^{(K)}\rangle$  for which the corresponding energy is less than a cut-off energy,  $E_{\text{cut}}$ .

To define the modified vibrational KEO, the full Hamiltonian

$$H = H_{\rm v} + T_{\rm vr} \tag{9}$$

is rewritten

$$H = \tilde{H}_{v} + \tilde{T}_{vr}, \tag{10}$$

by shifting a term from  $T_{\rm vr}$  into  $\tilde{H}_{\rm v}$ . Matrix elements of coordinate dependent factors in the terms of the KEO are integrals that are computed by quadrature. The KEO of the modified "vibrational" Hamiltonian is designed so that, if the primitive basis functions, used to solve eqn (8), are chosen correctly, all matrix elements of  $\tilde{H}_{v}$  in the primitive basis are finite. Some of the coordinate dependent factors in terms in  $\tilde{T}_{vr}$  are singular, but only where all wavefunctions have negligible amplitude. Such singularities are "unimportant". Some authors discard DVR or quadrature points close to an unimportant singularity, 5,6,31 but this is unnecessary. We find that for  $CO_2$ , points close to the  $\theta = 0$ singularity cause no problems. The KEO of eqn (1) is singular at the equilibrium geometry where  $\theta = \pi$  and also at  $\theta = 0$ . The  $\theta = 0$ singularity is unimportant because it corresponds to C-C-O which has a very high potential energy. The  $\theta = \pi$  singularity occurs in the factor  $\frac{1}{1+\cos\theta}$  in  $G_{zz}$ . To choose basis functions to deal with the important singularity, we use

$$\frac{1}{1+\cos\theta} = \frac{2}{\sin^2\theta} - \frac{1}{1-\cos\theta} \tag{11}$$

to rewrite

$$T_z = \frac{1}{2}G_{z,z}J_z^2$$

$$= \left[B_{R_1}(R_1) + B_{R_2}(R_2)\right] \left(\frac{1}{\sin^2 \theta} - \frac{1}{1 - \cos \theta}\right) J_z^2.$$
 (12)

The modified vibrational KEO and the corresponding modified ro-vibrational KEO are

$$\tilde{T}_{v} = T_{v} + \left[ B_{R_{1}}(R_{1}) + B_{R_{2}}(R_{2}) \right] \frac{J_{z}^{2}}{\sin^{2} \theta} 
\tilde{T}_{vr} = T_{vr} - \left[ B_{R_{1}}(R_{1}) + B_{R_{2}}(R_{2}) \right] \frac{J_{z}^{2}}{\sin^{2} \theta}.$$
(13)

In the shared-K associated Legendre function (ALF) basis  $\Theta_{i}^{K}(\theta)$ , the matrix elements of  $\tilde{T}_{v}$  are finite because

$$\left(-\frac{1}{\sin\theta}\frac{\partial}{\partial\theta}\sin\theta\frac{\partial}{\partial\theta} + \frac{J_z^2}{\sin^2\theta}\right)\Theta_l^K(\theta) = l(l+1)\Theta_l^K(\theta). \tag{14}$$

This two-step variational calculation method was first proposed by Tennyson and Sutcliffe9 and used to compute high-J levels of H<sub>2</sub>D<sup>+</sup>. The idea was subsequently used in many papers<sup>24–27,32–37</sup> to compute high-I levels of triatomic molecules. We compute the  $|v^{(K)}\rangle$  using the Lanczos algorithm.

Rather than using the two-step method, one could use a basis of products of J = 0 functions,  $|v^{(J=0)}\rangle$ , and symmetric top functions. In this basis, off-diagonal matrix elements,

$$\left\langle v'^{(J=0)} \left| \left\langle JKM \right| \left[ B_{R_1}(R_1) + B_{R_2}(R_2) \right] \frac{J_z^2}{\sin^2 \theta} \left| JKM \right\rangle \left| v^{(J=0)} \right\rangle \text{ are large.} \right.$$

In a two-step calculation, the term  $\left[B_{R_1}(R_1) + B_{R_2}(R_2)\right] \frac{J_z^2}{\sin^2 \theta}$ does not couple basis functions because it is included in the operator whose eigenfunctions are the  $|v^{(K)}\rangle$  basis functions.  $|v^{(K)}\rangle$  is like an eigenfunction of a 2-D harmonic oscillator with  $K = l_2$ . This basis includes all the bending states  $v_2^{l_2}(v_2=l_2,l_2+2,\cdots)$ . For a given  $K=l_2$ , the ground state of  $\tilde{H}_{v}$  is a state assigned to  $v_2 = l_2 = K$ .

# IV. Matrix elements in non-parityadapted bases

A. Matrix elements in the non-parity-adapted primitive basis The  $|v^{(K)}\rangle$  are computed for each *K* in a vibrational primitive basis

$$\left|v^{(K)}\right\rangle = \sum_{\alpha_1,\alpha_2} \sum_{l=K}^{K+l_x} c_{\alpha_1,\alpha_2,l,\nu}^K g_{\alpha_1}^{(1)}(R_1) g_{\alpha_2}^{(2)}(R_2) \Theta_l^K(\theta), \tag{15}$$

where  $\Theta_l^K(\theta)$  is an associated Legendre function (ALF) and  $g_{\alpha_1}^{(1)}(R_1)$ and  $g_{\alpha_2}^{(2)}(R_2)$  are discrete variable functions.<sup>17</sup> In this section we present equations for matrix elements in the primitive basis each of whose functions is a product of the vibrational functions in eqn (15) and a non-parity adapted rotational function,

$$g_{\alpha_1}^{(1)}(R_1)g_{\alpha_2}^{(2)}(R_2)\Theta_l^K(\theta)|JKM\rangle.$$
 (16)

Matrix elements in the basis of eqn (6) are obtained from those in this subsection by transforming. The range of l is  $[K,K+l_x]$ .  $l_x$  is the maximum value of l when K = 0. In the following, the bendrotation part of this basis function is denoted (dropping M)

$$|l;J,K\rangle = \Theta_l^K(\theta)|JKM\rangle.$$
 (17)

In the basis of eqn (16) the matrix representing  $\tilde{T}_{\rm v}$  is diagonal and its elements are

$$\langle l'; J, K | \tilde{T}_{v} | l; J, K \rangle = [B_{R}(R_1) + B_{R_2}(R_2)] l(l+1) \delta_{l',l}.$$
 (18)

The matrix elements of the ro-vibrational term  $\tilde{T}_{\rm vr}$  in the primitive basis are,

$$\langle l'; J, K | \tilde{T}_{vr} | l; J, K \rangle = \left[ B_{R_1}(R_1) + B_{R_2}(R_2) \right] \left[ \left( \frac{1}{8} \delta_{l',l} + \frac{1}{4} I_{l',l,K} \right) \right] \times J(J+1) - \left( \frac{1}{8} \delta_{l',l} + \frac{3}{4} I_{l',l,K} \right) K^2 \right]$$
(19)

 $\langle l'; J, K+1 | \tilde{T}_{vr} | l; J, K \rangle$ 

$$= \frac{1}{4} \lambda_{J,K}^{+} \left[ B_{R_1}(R_1) - B_{R_2}(R_2) \right] \left[ (2K+1) \left( G_{l',l,K} + D_{l',l,K} \right) + 2\lambda_{l,K}^{+} \delta_{l',l} \right]$$
(20)

$$\langle l'; J, K+2 | \tilde{T}_{vr} | l; J, K \rangle = \frac{1}{16} \lambda_{J,K}^{+} \lambda_{J,K+1}^{+} \times \left[ B_{R_1}(R_1) + B_{R_2}(R_2) \right] \left( 2J_{l',l,K} - H_{l',l,K} \right), \tag{21}$$

 $\lambda_{J,K}^+ = \sqrt{J(J+1) - K(K+1)}$ . The matrices **D**, **G**, **H**, **I** and **J** are given in Appendix A of ref. 30. They are reproduced below,

$$D_{l',l,m} = \langle \Theta_{l'}^{m+1} | \cot \theta | \Theta_{l}^{m} \rangle.$$

$$G_{l',l,m} = \langle \Theta_{l'}^{m+1} | \frac{1}{\sin \theta} | \Theta_{l}^{m} \rangle$$

$$H_{l',l,m} = \langle \Theta_{l'}^{m+2} | \Theta_{l'}^{m} \rangle$$

$$I_{l',l,m} = \langle \Theta_{l'}^{m} | \frac{1}{1 - \cos \theta} | \Theta_{l'}^{m} \rangle$$

$$J_{l',l,m} = \langle \Theta_{l'}^{m+2} | \frac{1}{1 - \cos \theta} | \Theta_{l'}^{m} \rangle.$$
(22)

All these matrices can be computed numerically exactly with a Gauss Legendre quadrature except for **I**. See ref. 30 for details. When K=0, matrix elements of **I** are singular at  $\theta=0$ . However, this singularity is unimportant because of the high potential at  $\theta=0$ . One only needs accurate integrals in the region of configuration space in which wavefunctions are not negligible.<sup>38</sup> The matrix elements in eqn (18)–(21) have been given in ref. 30, where the bisector-z KEO (the bisector-x KEO was not used) was used to compute the spectrum of an  $H_2O$ -atom complex, but in the second equation of eqn (28) of ref. 30, there is a sign error:  $-2\lambda_{LK}^{+}\delta_{l',l}$  should be  $+2\lambda_{LK}^{+}\delta_{l',l}$ .

Note that  $\mathbf{G} + \mathbf{D}$  could be combined into one matrix by computing matrix elements of  $(1 + \cos \theta)/\sin \theta$  and that  $2\mathbf{J} - \mathbf{H}$  could be combined into one matrix by computing matrix elements of  $(1 + \cos \theta)/(1 - \cos \theta)$ . We have not made these combinations because we want to give the matrix elements that

are required for both the bisector-z and the bisector-z frames.<sup>30</sup> Specifically, for the bisector-z frame,  $\mathbf{G} - \mathbf{D}$  is the matrix representing  $(1 - \cos \theta)/\sin \theta$  and it appears in  $\Delta K = 1$  matrix elements, and  $2\mathbf{F} - \mathbf{H}$  is the matrix representing  $(1 - \cos \theta)/(1 + \cos \theta)$  and it appears in  $\Delta K = 2$  matrix elements.<sup>30</sup>

As noted after eqn (16), the maximum of l for the ALF basis is extended from  $l_x$  to  $K + l_x$ . This ensures that the bend basis size,  $l_x + 1$ , is the same for each K since the minimum value of l is K. As a result, the quality of the converged vibrational levels is maintained for all K. Note, however, that as K becomes larger, fewer  $|\nu^{(K)}\rangle$  are retained because fewer of the corresponding energies are below  $E_{\text{cut}}$ . When J is much smaller than  $l_x$ , it is fine to set the maximum value of l at  $l_x$ . For each K, the integration over  $\theta$ , required to calculate matrix elements of the potential, is done with at least  $N_{\theta} = K + l_x + 1$  Gauss Legendre quadrature points. In fact, we use the same  $J_x + l_x + 1$  Gauss Legendre quadrature points for all K,  $J_x$  is the largest J. Using one set of points instead of a different set for each K gives us the advantage of needing to compute and store potential points only once. It would also be possible to use a K dependent Gauss Jacobi quadrature with only  $l_r + 1$  points (for each K), for which the points are determined by diagonalizing  $\cos \theta$  in a ALF basis. If we used these points we would be doing a finite basis representation (FBR) calculation equivalent to the DVR calculation of DVR3D. Both quadratures allow one to evaluate potential matrix vector products with the sequential summation technique and use an iterative eigensolver to compute thousands of eigenstates  $|v^{(K)}\rangle$  directly in the 3D direct product primitive basis. The 3-D direct product basis is large, but that is not a problem if an iterative eigensolver is used. If a direct eigensolver used, it is common to reduce the size of the primitive basis by doing a series of diagonalizations and truncations. 5,6,27,33

#### B. Matrix elements in the non-parity-adapted contracted basis

Using the  $\tilde{T}_{vr}$  matrix elements in Section IVA, it is straightforward to compute the matrix elements of the ro-vibrational Hamiltonian in the contracted basis. The diagonal elements are

$$\langle v'; J, K | H | v; J, K \rangle = \mathcal{E}_{v}^{(K)} \delta_{v',v} + J(J+1) \left( X_{v',v}^{K} + Y_{v',v}^{K} \right) - K^{2} \left( X_{v',v}^{K} + 3 Y_{v',v}^{K} \right).$$
(23)

The matrix elements off-diagonal in K are

$$\langle v'; J, K+1|H|v; J, K \rangle = \lambda_{J,K}^{+} Z_{v',v}^{K}$$
 (24)

$$\langle v'; J, K + 2|H|v; J, K \rangle = \lambda_{J,K}^{+} \lambda_{J,K+1}^{+} W_{v',v}^{K},$$
 (25)

where

$$|\nu;J,K\rangle \equiv |\nu^{(K)}\rangle |J,K\rangle$$
 (26)

$$X_{\nu',\nu}^{K} = \frac{1}{8} \sum_{\alpha_{1},\alpha_{2}} \sum_{l=K}^{K+l_{x}} c_{\alpha_{1},\alpha_{2},l,\nu'}^{K} c_{\alpha_{1},\alpha_{2},l,\nu}^{K} \left[ B_{R_{1}} \left( R_{\alpha_{1}} \right) + B_{R_{2}} \left( R_{\alpha_{2}} \right) \right]$$
 (27)

$$Y_{\nu,\nu}^{K} = \frac{1}{4} \sum_{\alpha_{1},\alpha_{2}} \sum_{l',l=K}^{K+l_{x}} c_{\alpha_{1},\alpha_{2},l',\nu'}^{K} c_{\alpha_{1},\alpha_{2},l,\nu}^{K} \left[ B_{R_{1}} \left( R_{\alpha_{1}} \right) + B_{R_{2}} \left( R_{\alpha_{2}} \right) \right] I_{l',l,K}$$

$$(28)$$

$$Z_{\nu',\nu}^{K} = \frac{1}{4} \sum_{\alpha_{1},\alpha_{2}} \sum_{l'=K+1}^{K+1+l_{x}} \sum_{l=K}^{K+l_{x}} c_{\alpha_{1},\alpha_{2},l',\nu'}^{K+1} c_{\alpha_{1},\alpha_{2},l,\nu}^{K} \left[ B_{R_{1}}(R_{\alpha_{1}}) - B_{R_{2}}(R_{\alpha_{2}}) \right]$$

$$\times \left[ (2K+1) \left( G_{l',l,K} + D_{l',l,K} \right) + 2\lambda_{l,K}^{+} \delta_{l',l} \right]$$
(29)

$$W_{v',v}^{K} = \frac{1}{16} \sum_{\alpha_{1},\alpha_{2}} \sum_{l'=K+2}^{K+2+l_{x}} \sum_{l=K}^{K+l_{x}} c_{\alpha_{1},\alpha_{2},l',v'}^{K+2} c_{\alpha_{1},\alpha_{2},l,v}^{K} \left[ B_{R_{1}} \left( R_{\alpha_{1}} \right) + B_{R_{2}} \left( R_{\alpha_{2}} \right) \right]$$

$$\times (2J_{l',l,K} - H_{l',l,K}). \tag{30}$$

Although it is not indicated, the indices  $\nu$  and  $\nu'$  in X and Y depend on K. The index v' in **Z** depends on K + 1, and the index v' in **W** depends on K + 2. Note that **X**, **Y**, **Z**, and **W** are independent of J. They are evaluated for  $K = 0, 1, ..., K_{\text{max}}$  and stored on disk in the first step. They are used in the second step calculation for all *J*.  $K_{\text{max}} \leq J$ , but for high J calculations,  $K_{\text{max}}$  can be much smaller than J, eliminating the cost of calculating  $v^{(K)}$  when K is between  $K_{\text{max}}$  and J.

# V. Parity symmetry and O-O permutation symmetry

#### A. Parity symmetry

To utilize the parity symmetry, we note that the parity operator does not affect the vibrational coordinates, but affects the rotational coordinates for the molecule-fixed frame we use,

$$E^*(R_1, R_2, \theta; \alpha, \beta, \gamma) = (R_1, R_2, \theta; \pi + \alpha, \pi - \beta, \pi - \gamma). \tag{31}$$

As a result,

$$E^*|JK\rangle = (-1)^{J+K}|J\bar{K}\rangle$$

$$E^*|I,JK\rangle = (-1)^J|I,J\bar{K}\rangle.$$
(32)

 $\bar{K} = -K$ . The parity-adapted (PA) primitive basis is therefore

$$g_{\alpha_{I}}^{(1)}(R_{1})g_{\alpha_{2}}^{(2)}(R_{2})\Theta_{I}^{K}(\theta)R_{IK}^{P},$$
 (33)

where

$$R_{JK}^{P} = N_{K} \frac{1}{\sqrt{2}} \left[ |JK\rangle + (-1)^{J+K+P} |J\bar{K}\rangle \right], \tag{34}$$

with  $N_K = (1 + \delta_{K,0})^{-1/2}$ . P = 0 and 1 correspond to even and odd parity, respectively, and  $K \ge 0$  for  $(-1)^{l+p} = 1$  and  $K \ge 1$  for  $(-1)^{l+p} = -1$ .  $(-1)^{J+P} = \pm 1$  is called the spectroscopic parity e/f and is a popular label for linear molecules.  $R_{IK}^{P}$  is an eigenfunction of  $E^{*}$ 

$$E^*R_{IK}^P = (-1)^P R_{IK}^P. \tag{35}$$

Matrix elements of rotational operators in the  $R_{JK}^P$  basis are given for example in ref. 39. They will be used to derive the KEO matrix elements in the PA primitive basis. We denote the angular part of the PA primitive basis by

$$|l;J,K,P\rangle = \Theta_l^K(\theta)R_{lK}^P. \tag{36}$$

Although the PA primitive basis for a triatomic is a product of a vibrational factor and rotational factor,

this is not the case for molecules with more than three atoms.

#### O-O permutation symmetry

The O-O permutation symmetry operator (12) permutes atoms  $O_1$  and  $O_2$ . The bisector-x frame is affected by (12) because the x-axis is unchanged and the y- and z-axes are flipped. The effect of (12) on the ro-vibrational coordinates is

$$(12)(R_1, R_2, \theta; \alpha, \beta, \gamma) = (R_2, R_1, \theta; \pi + \alpha, \pi - \beta, -\gamma).$$
 (37)

As a result,

$$(12)|JK\rangle = (-1)^{J}|J\bar{K}\rangle$$

$$(12)|l,JK\rangle = (-1)^{J+K}|l,J\bar{K}\rangle$$

$$(12)R_{JK}^{P} = (-1)^{K+P}R_{JK}^{P}.$$
(38)

## VI. Matrix elements in parity-adapted bases

#### A. Matrix elements in the parity-adapted primitive basis

The matrix elements of  $\tilde{T}_{v}$  in the PA primitive basis are the same as those in the primitive basis. Matrix elements of  $\tilde{T}_{vr}$  in the PA primitive basis are the same as those in the primitive basis except each is multiplied by a factor,  $F_K = (1 + \delta_{K,0})^{1/2}$ . They can be derived by taking advantage of the factorization in eqn (36) and using the matrix elements of rotational operators in the  $R_{JK}^P$  basis given in ref. 39. The results are

$$\langle l';J,K,P|\tilde{T}_{v}|l;J,K,P\rangle = [B_{R_{1}}(R_{1}) + B_{R_{2}}(R_{2})]l(l+1)\delta_{l',l}$$
(39)
$$\langle l';J,K,P|\tilde{T}_{vr}|l;J,K,P\rangle = [B_{R_{1}}(R_{1}) + B_{R_{2}}(R_{2})] \left[ \left( \frac{1}{8}\delta_{l',l} + \frac{1}{4}I_{l',l,K} \right) \times J(J+1) - \left( \frac{1}{8}\delta_{l',l} + \frac{3}{4}I_{l',l,K} \right) K^{2} \right]$$
(40)

$$\langle l'; J, K+1, P | \tilde{T}_{vr} | l; J, K, P \rangle = \frac{F_K}{4} \lambda_{J,K}^+ \left[ B_{R_1}(R_1) - B_{R_2}(R_2) \right]$$

$$\times \left[ (2K+1) \left( G_{l',l,K} + D_{l',l,K} \right) \right]$$

$$+ 2\lambda_{l,K}^+ \delta_{l',l}$$
(41)

$$\langle l'; J, K+2, P | \tilde{T}_{vr} | l; J, K, P \rangle = \frac{F_K}{16} \lambda_{J,K}^+ \lambda_{J,K+1}^+ \left[ B_{R_1}(R_1) + B_{R_2}(R_2) \right] \left( 2J_{l',J,K} - H_{l',J,K} \right).$$
(42)

There is an additional special diagonal matrix element of  $\tilde{T}_{\rm vr}$ for K = 1 arising from  $J_x^2 - J_y^2$  (there is no corresponding matrix element in the non-PA basis),

$$\langle l'; J, 1, P | \tilde{T}_{vr} | l; J, 1, P \rangle = \frac{1}{16} [B_{R_1}(R_1) + B_{R_2}(R_2)]$$
  
  $\times J(J+1)(-1)^{J+P} (\delta_{l',l} - 2I_{l',l,1}).$ 

#### B. Matrix elements in the parity-adapted contracted basis

A PA contracted basis function is

$$|\nu;J,K,P\rangle = |\nu^{(K)}\rangle R_{LK}^{P}.$$
 (43)

The matrix elements of the ro-vibrational Hamiltonian in the PA contracted basis are the same as those in the contracted basis, eqn (23)–(30), except that the K-off-diagonal elements have an  $F_K$  factor,

$$\langle v'; J, K, P | H | v; J, K, P \rangle = \mathcal{E}_{v}^{(K)} \delta_{v', v} + J(J+1) \left( X_{v', v}^{K} + Y_{v', v}^{K} \right)$$
$$- K^{2} \left( X_{v', v}^{K} + 3 Y_{v', v}^{K} \right)$$
(44)

$$\langle v'; J, K+1, P|H|v; J, K, P\rangle = F_K \lambda_{J,K}^+ Z_{v',v}^K$$
 (45)

$$\langle v'; J, K+2, P|H|v; J, K, P\rangle = F_K \lambda_{J,K}^+ \lambda_{J,K+1}^+ W_{v',v}^K,$$
 (46)

and there is a special diagonal matrix element for K = 1,

$$\langle v'; J, 1, P | \tilde{T}_{vr} | v; J, 1, P \rangle = \frac{1}{2} J(J+1)(-1)^{J+P} \left( X_{v',v}^1 - Y_{v',v}^1 \right).$$
 (47)

Note that there are two differences between the even and odd parity Hamiltonian matrices: (i) the K=1 diagonal elements are different due to eqn (47); and (ii) when  $(-1)^{J+P}=1$ , the matrix has an additional K=0 row and column. In the vector-z frame case, there are no special elements and the even and odd matrices differ only because when  $(-1)^{J+P}=1$  there is an additional K=0 row and column.

## VII. Comparison with other methods

Many variational methods for computing energy levels of triatomic molecules exist. What is unique about the method we propose in this paper? Most variational methods have four basic components: (i) coordinates; (ii) primitive and contracted basis functions; (iii) matrix elements; (iv) a method for computing eigenvalues and eigenvectors of the Hamiltonian matrix. There are no papers using the combination of (i), (ii), (iii), and (iv) that we use suggest in this paper. Our combination is straightforward to implement and has advantages. In this section we compare our approach to approaches of other groups.

Carter and Handy (CH) were the first to use the bisector-x frame KEO in their calculation of energy levels of  $\rm H_2O^{32}$  and later of HCN. They also use the two-step method. Their coordinates are bond lengths and the bond angle. There is less potential coupling in bond coordinates than in Radau coordinates, but more kinetic coupling (the vibrational KEO has cross terms between the stretch coordinates and between stretch coordinates and the bend coordinate and additional ro-vibrational terms). The Radau KEO we use has fewer terms. CH used 1-D contracted basis functions and an optimised quadrature scheme. Instead, we use tridiagonal Morse DVR functions for the stretches and ALF functions for the bend. CH did not publish equations for

the matrix elements in the ALF basis. They use a direct eigensolver, which limits the size of the primitive basis they can use

Tennyson and co-workers<sup>5,6</sup> use the same bisector-x frame KEO, the same Radau coordinates, and a two-step method as we do in this paper. Their approach is implemented in the DVR3D code<sup>5,6</sup> used in many calculations of triatomic molecules. Their method differs from ours in the choice of the primitive basis. To compute  $|\nu^{(K)}\rangle$ , they use K-dependent DVR functions for the bend coordinate and we use ALF functions. The DVR3D bend basis functions are

$$\left|\gamma^{K}\right\rangle = \sum_{l=K}^{l=K+l_{x}} T_{l,,K}^{K} \Theta_{l}^{K}(\theta). \tag{48}$$

where  $T_{l,\gamma^K}^K$  is a transformation matrix determined by diagonalizing the matrix representing  $\cos \theta$  in the ALF basis. <sup>17</sup> Because we do not use a DVR for  $\theta$ , we must evaluate integrals by quadrature. If we used the Gauss-Jacobi quadrature that underlies the K-dependent DVR used in DVR3D, then our Hamiltonian matrix and the matrix of DVR3D would be unitarily equivalent,  $\mathbf{H}^{\mathbf{DVR3D}} = (\mathbf{T}^{\mathbf{K}})^{\mathbf{T}} \tilde{\mathbf{H}}_{\mathbf{v}} \mathbf{T}^{\mathbf{K}}$ , where  $\tilde{\mathbf{H}}_{\mathbf{v}}$  is the matrix computed with Gauss-Jacobi quadrature. Instead, we use a Kindependent quadrature. 17 DVR3D computes matrices representing coordinate dependent factors D, G, H, I, and J, in the ALF basis and then transforms them to the K-dependent DVR. By using only the ALF, we obviate the need to transform all these matrices into the DVR. The transformation is a bit tricky because the DVR is K-dependent which means that different transformation matrices must be used on the left and on the right. In Section 2.3 of ref. 42, it is noted that the cost of transforming into the DVR can be reduced by doing sums sequentially; we completely eliminate the transformation. In the first two-step paper<sup>9</sup> in 1986, a vector-z frame and an ALF basis were used. DVR3D uses not only a different primitive basis but also a different contracted basis. As pointed out by Yan, Xie and Tian,34 in the two-step calculation of DVR3D, the contracted functions computed in the first step are different for each J, K pair. The modified "vibrational" KEOs used by DVR3D and by Carter and Handy<sup>32</sup> include not only  $\tilde{T}_{v}$ , but also all  $J^{2}$ and  $I_z^2$  terms. In other words, they added the second and third terms on the RHS of eqn (23). We find that most of the computation time is spent in the first-step of the calculation. If, as is true in our calculation, it is not necessary to recompute  $|v^{(K)}\rangle$  for each value of J, a lot of computer time is saved. Another difference between DVR3D and what we do is that we do not discard quadrature points close to the singularity.

The most accurate  $CO_2$  calculations have been done with a method developed by Schwenke and co-workers.  $^{25-27,35}$  It is quite different from our approach. They use different molecule-fixed axes, a different contraction scheme, and a direct eigensolver. They first contract together bend and rotation, then they contract their bend-rotation functions with a 1-D contracted antisymmetric stretch basis, finally they contract their bend-rotation-antisymmetric stretch functions with 1-D contracted symmetric stretch functions. They used the vector-z BF frame.

Matrix elements off-diagonal in K are larger in the vector-z frame than in the bisector-x frame, but that coupling is accounted for in the first contraction and therefore not a problem. Schwenke and co-workers cannot use a symmetryadapted primitive basis to set up their bend-rotation matrix because permuting the two O atoms changes their primitive functions (because they use the vector-z frame) in a complicated way. However the bend-rotation contracted functions are symmetric or antisymmetric under O-O permutation. They assign permutation symmetry labels to their bend-rotation contracted functions by analysing the functions at a set of points (see ref. 43). These symmetry-labelled bend-rotation contracted functions are then coupled to the symmetrylabelled contracted antisymmetric stretch functions to form the final symmetry-labelled basis functions. A disadvantage of their contraction scheme is that the important coupling between bend and symmetric stretch basis function is incorporated at the end of the calculation. On the other hand, an advantage is it can be used on molecules with more than three atoms. Everything is implemented in their VTET code. Their bend-rotation functions are similar to the rigid-bender functions of Bunker44 and to the bend-rotation functions used for methane in ref. 45. Schwenke et al. used an optimised quadrature scheme<sup>40,41</sup> to compute matrix elements in their contracted basis. The nested contraction scheme makes it possible to calculate accurate ro-vibrational levels up to I =150 and levels higher than 20 000 cm<sup>-1</sup> were converged. In this paper, we use their levels, 27,46 called Huang2022 levels, as a benchmark to compare with our levels. The levels we received from them are published in ref. 27 and are used to generate the Ames-2021 line list.<sup>27</sup> We also compare with their levels computed with a smaller basis on the same PES26 and call them Huang2017 levels.

Yurchenko and Mellor<sup>28,47</sup> propose a TROVE method to compute ro-vibrational levels and wavefunctions of CO<sub>2</sub>. They also used the bisector-x frame and their treatment of the KEO is exact. However, they represent the potential with a 12th order Taylor expansion. They compared their energies with those computed with DVR3D24 on an earlier Ames-1 PES25 rather than the Ames-2 PES<sup>26</sup> we are using. (They mistakenly stated that they used the Ames-2 PES.) Errors appear to be due to the Taylor series approximation. The largest error in their Table 1 is  $0.0335 \text{ cm}^{-1} \text{ for a } I = 0 \text{ DVR3D level at } 5667.6298 \text{ cm}^{-1}. \text{ The}$ error of our calculation for this level is less than  $1 \times 10^{-5}$  cm<sup>-1</sup>.

The two-step method with the ALF basis that is explained in this paper has been added to our RV3 code. 48 The code computes the ro-vibrational energy levels, wavefunctions, and intensities of a three-atom molecule using a variety of basis functions including non-contracted bases, e.g. ALF and DVR

Table 1 Calculation parameters for CO<sub>2</sub>

 $m_{\rm (C)} = 21\,868.66175734604622 \ m_{\odot}$  $m_{(O)} = 29148.94559967216628 m_e$ 1 Hartree = 219 474.631482453 cm<sup>-1</sup>  $a_0 = 0.529177249 \text{ Å}$ 

bend bases, and contracted bases, e.g. a shared-K contracted basis  $|v(K)\rangle|JKM\rangle$  (this work) a non shared-K contracted basis  $|\nu\rangle|IKM\rangle$ . <sup>38</sup> All these bases can be used with the vector-z frame, the bisector-x frame, the bisector-z frame and the Eckart frame.

#### VIII. Results

The highly accurate Ames-2 PES<sup>26</sup> was used in all calculations. The masses and constants are given in Table 1.46

#### A. Primitive basis optimization and primitive-basis convergence tests

We use a tridiagonal Morse(TDM) DVR basis for the stretch coordinates  $R_1$  and  $R_2$ . Compared to a basis of Morse wavefunctions, it has the advantage that it is possible to define a corresponding DVR. 49 The TDM basis depends on the values of parameters that appear in a Morse potential:  $D_e$ ,  $\omega_e$ , and  $R_e$ , and on a fourth parameter that is called  $\gamma$  in ref. 49 and  $\alpha$  in ref. 50 and 51;  $\alpha = 2\gamma$ . Here we use the  $\alpha$  notation. The superscript of the associated Laguerre polynomials  $L_n^{\alpha}(y)$  in the TDM function is  $\alpha$ . It is chosen as in ref. 49, so that the TDM basis spans the same space as the [A/2] bound states of the Morse oscillator.  $D_e$ ,  $\omega_e$ , and  $R_e$  are optimized to minimize low-lying J = 0 levels. For the optimization,  $l_x$  is fixed at 50 which is more than enough for levels up to 10 000 cm<sup>-1</sup>. A large (120) sine DVR basis provides the benchmark for the optimization. Our final parameters for the TDM basis are  $D_e = 65\,000 \text{ cm}^{-1}$ ,  $\omega_e = 2170 \text{ cm}^{-1}$ ,  $R_e =$ 2.14 $a_0$ .  $A = 4D_e/\omega_e = 119.82$ . The number of Morse bound states is [A/2] = 59. According to ref. 49,  $\alpha = A - 2[A/2] = 1.82$ , if  $N_{R_i} \ge$ 59; and  $\alpha = A - 2N_{R_i}$  if  $N_{R_i} \le 59$ .

We determine the size of the primitive ALF basis,  $l_x$ , by doing calculations with a small TDM basis. Our goal is to converge energy levels up to 20 000 cm<sup>-1</sup> with errors of  $1 \times 10^{-4}$  cm<sup>-1</sup>. We fix  $N_{R_1} = N_{R_2} = 28$  and find that  $l_x = 150$  is enough to converge levels up to 20 000 cm<sup>-1</sup> to within  $3 \times 10^{-5}$  cm<sup>-1</sup>, by comparing with levels computed with  $l_x$  = 200. Subsequently, with  $l_x$  = 150 fixed, we test TDM DVR bases with up to  $N_{R_1} = N_{R_2} = 80$ . The basis with  $(N_{R_1} = N_{R_2}, l_x) = (50, 150)$  is chosen as our final primitive basis and is hereafter called basis I. Compared to levels computed with  $(N_{R_1} = N_{R_2}, l_x) = (80, 150)$ , basis I converges almost all the J = 0 levels up to 20000 cm<sup>-1</sup> to within 1 ×  $10^{-4} \, \text{cm}^{-1}$ ; the largest error is 0.00165 cm<sup>-1</sup> at 19160 cm<sup>-1</sup>. We refer to the difference between levels computed with the  $(N_{R_1} =$  $N_{R_1}, l_x$  = (50, 150) basis and with the  $(N_{R_1} = N_{R_2}, l_x)$  = (80, 150) basis as the primitive-basis error see Table 2. Basis I has 377 500 functions, for J = 0.

We have used the same masses and constants as those used by Huang et al. 26,27 Nonetheless, there are still small differences between our levels and the levels of Huang2017 and Huang2022, for low-lying levels that should be fully converged in both calculations. For example, for levels up to 3000 cm<sup>-1</sup>, the largest difference is 0.0003 cm<sup>-1</sup> for the level at 2548.36615 cm $^{-1}$  (see Table S1 of ESI $^{\dagger}$ <sup>52</sup>). This difference is certainly not due to convergence error in either calculation. We therefore consider any differences larger than 0.0003 cm<sup>-1</sup> to

**Table 2** Testing the convergence of primitive vibrational bases.  $A_{15k}/A_{20k}$  are the maxium absolute differences for the A+ symmetry J=0 vibrational levels up to  $15\,000/20\,000~{\rm cm}^{-1}$ , respectively, relative to the benchmark results obtained with the primitive basis  $N_{R_1}=N_{R_2}=80$  and  $I_x=150$ . The energies are in cm<sup>-1</sup>. The number of bend quadrature points is  $N_{\theta}=I_x+1$ 

$(N_{R_1}=N_{R_2},l_x)$	$N_{ m bas}$	$\it \Delta_{15k}$	$\varDelta_{20\mathrm{k}}$
(32, 120)	108 900	0.00669	8.188
(32, 150)	154 624	0.00022	0.04900
(50, 150)	377 500	0.00003	0.00165
(60, 150)	543 600	0.00003	0.00027
(80, 150)	966 400	0	0
Huang2017		0.00029	0.07551
Huang2022		0.00102	0.00116

be due to their basis set convergence error. In Table 2, we show that, for J=0 levels below 20 000 cm $^{-1}$ , the largest difference is 0.00116 cm $^{-1}$  comparing to the Huang2022 levels and 0.07551 cm $^{-1}$  comparing to the Huang2017 levels. The largest differences are in bold in Table S1 of ESI.† $^{52}$  This indicates that there are small convergence errors in their J=0 levels. A list of all the J=0 A+ levels is given in Table S1 of the ESI.† $^{52}$ 

We could also compare levels computed with our primitive basis and those of Zak *et al.*,  $^{24}$  who used 30 slightly different TDM DVR basis functions for the stretches and  $l_x$  = 120 and a different PES (Ames-1 PES). To estimate convergence errors of their calculation, we have determined that (using our TDM functions) the  $(N_{R_1} = N_{R_2}, l_x) = (30, 120)$  basis gives errors as large as 0.00669 cm<sup>-1</sup> up to 15 000 cm<sup>-1</sup> and as large as 8.188 cm<sup>-1</sup> up to 20 000 cm<sup>-1</sup>. However, the goal of Zak *et al.* was to compute levels only up to 14 500 cm<sup>-1</sup> see Table 2.

#### B. Convergence of energies computed in the contracted basis

When J is large, rather than using the primitive basis, we use the contracted basis. The primitive basis of the previous paragraph (basis I) is used to compute the contracted basis functions. The convergence of the second step of the two-step calculation depends on the cut-off energy  $E_{\rm cut}$  used to determine the size of the  $v^{(K)}$  basis. As  $E_{\text{cut}}$  is increased, levels of the two-step calculations approach those computed in the primitive basis used to compute the  $v^{(K)}$ . We can therefore use a calculation done in the primitive basis to test the convergence of the two-step calculation, at least when I is not too large. The calculation with the primitive basis is much more costly than the two-step calculation. To compare the primitive (basis I) and 2-step levels, we use the J = 20 A + symmetry levels up to20 000 cm<sup>-1</sup>. The primitive basis has 8 452 500 even-parity basis functions see Table 3 for details. We find that the contracted basis with  $E_{\text{cut}} = 30\,000 \text{ cm}^{-1}$  is sufficient to converge levels up to 20 000 cm $^{-1}$  to within 3.4  $\times$  10 $^{-5}$  cm $^{-1}$  see column 5 and 6 of Table 3. We therefore use  $E_{\text{cut}} = 30\,000 \text{ cm}^{-1}$  to compute all the levels reported in this paper, up to J = 100.

Errors in the final energy levels can be caused by using a primitive basis and/or a  $E_{\rm cut}$  that is too small. We estimate that the total error in the levels we report is about 0.0001 cm<sup>-1</sup>, for all levels up to 20 000 cm<sup>-1</sup>. If one aims to converge only levels up to 15 000 cm<sup>-1</sup>, one can lower  $E_{\rm cut}$  to at least 25 000 cm<sup>-1</sup>. When  $E_{\rm cut}$  is large enough, the error in two-step eigenvalues

**Table 3** Testing the convergence of the two-step calculations with respect to the cutoff energy  $E_{\rm cut}$ . The J=20 A+ symmetry rovibrational levels up to 20 000 cm $^{-1}$  (the number of levels is 2151) are used to do the test.  $\Delta_{\rm 15k}/\Delta_{\rm 20k}$  are the maxium absolute differences up to 15 000/20 000 cm $^{-1}$ , respectively, relative to the benchmark levels computed in the  $N_{R_1}=N_{R_2}=50$ ,  $l_{\rm x}=170$  primitive basis with  $N_{\theta}=171$  and relative to two-step levels computed with  $E_{\rm cut}=38\,000$  cm $^{-1}$ . The size of the even-parity primitive basis is 8 452 500. The energies are in cm $^{-1}$ 

		Relative to $E_{\text{cut}} = 38000$		Relative to the benchmark		
$E_{ m cut}$	$N_{ m bas}$	$\Delta_{15\mathrm{k}}$	$\varDelta_{20k}$	$\varDelta_{15k}$	$\varDelta_{20k}$	
38 000	21 428	0.0	0.0	$2.2 \times 10^{-5}$	$3.4 \times 10^{-5}$	
30 000	9185	$2.0 \times 10^{-9}$	$2.8 \times 10^{-6}$	$2.2 \times 10^{-5}$	$3.4 \times 10^{-5}$	
27 000		$8.2 \times 10^{-8}$		$2.2 \times 10^{-5}$	0.00016	
26 000	5513	$3.1 \times 10^{-7}$		$2.2 \times 10^{-5}$	0.00085	
25 000	4809	$1.7 \times 10^{-6}$		$2.2 \times 10^{-5}$	0.00227	
23 000	3581	$1.5 \times 10^{-5}$	0.06602	$2.2 \times 10^{-5}$	0.06602	
Huang2022	2 N/A	0.00208	0.01966	0.00210	0.01966	

compared to the corresponding primitive-basis eigenvalues decreases quickly as  $E_{\rm cut}$  is increased. However, this two-step error is not the only error, there is also the primitive-basis error. For J=20~A+, see Table 3, the largest eigenvalue difference between two-step calculations with  $E_{\rm cut}=30~000~{\rm cm}^{-1}$  and  $E_{\rm cut}=15~000~{\rm cm}^{-1}$  is  $\Delta_{15\rm k}=2.0\times10^{-9}~{\rm cm}^{-1}$ , but this does not imply that errors in two-step eigenvalues computed with  $E_{\rm cut}=15~000~{\rm cm}^{-1}$  are  $2.0\times10^{-9}~{\rm cm}^{-1}$  because there is also primitive-basis error. In fact, the largest difference between two-step levels with  $E_{\rm cut}=15~000~{\rm cm}^{-1}$  and primitive-basis levels computed with the larger primitive basis  $(N_{R_1}=N_{R_2}I_x)=(50,~180)$  primitive basis is  $2.2\times10^{-5}~{\rm cm}^{-1}$ . When J is large, primitive-basis levels with the  $(N_{R_1}=N_{R_2}I_x)=(50,~180)$  basis are not available. Convergence with respect to  $E_{\rm cut}$  is not the full story.

Many researchers, such as Carter and Handy,  $^{32,33}$  Zak *et al.*,  $^{24}$  Zuniga *et al.*,  $^{36,37}$  use a fixed number of  $v^{(K)}$  functions for each K. This number is often called N. For a given J, this corresponds to Hamiltonian matrices of size N(J+1) and NJ for  $(-1)^{J+P}=1$  and -1, respectively. To limit the size of the matrices in the final diagonalization, it is common to use a smaller N when J is large. E.g., Zak *et al.*  $^{24}$  use N=600 for J=0-50 and N=100 for J=87-129.

Instead, we use  $E_{\text{cut}}$  to determine the number of  $v^{(K)}$ functions for each K. According to perturbation theory, the importance of coupling between zeroth-order states  $v^{(K)}$  and  $v^{\prime(K')}$  depends on the difference between their (zeroth-order) energies. Ecut therefore seems like a good criterion for determining the number of  $v^{(K)}$  to retain.  $E_{\text{cut}}$  is also used in the work of Schwenke and co-workers. 25-27 For each symmetry block, the number of  $v^{(K)}$  we retain, denoted by N(K), decreases with K, because the corresponding energies are larger when K is larger see Table 4.  $A\pm$  levels ( $B\pm$  levels are Pauli forbidden) are computed from a basis of products of  $A\pm$  ( $B\pm$ ) rotational functions  $R_{JK}^P$  and A+ (B+)  $v^{(K)}$  functions. Because the A/Bsymmetry of the rotational functions  $R_{JK}^P$  alternates with K(see eqn (38)), the symmetry of  $v^{(K)}$  must also alternate. We choose  $E_{\text{cut}} = 30\,000 \text{ cm}^{-1}$  in our final calculations and for a  $(-1)^{J+P}$  = 1 calculation, N(K) is 885(A), 685(B), 787(A), 601(B) for K = 0, 1, 2, 3, respectively. It is 1(B), 3(A), 0(B), 1(A) for K = 39, 40,

**Table 4** The number of  $v^{(K)}$  functions, N(K), with energies under  $E_{cut} =$  $30\,000~{\rm cm}^{-1}$  with symmetry A+ and B+. The last column is the energy of the lowest state for each K, which corresponds to  $v_2 = K$  and  $l_2 = K$ . The energies are relative to the ZPE of 2535.79929 cm<sup>-1</sup>

K	N(K)(A+)	N(K)(B+)	Energy
0	885	733	0.000
1	832	685	668.151
2	787	645	1338.251
3	737	601	2010.299
4	692	564	2684.298
5	647	526	3360.249
6	606	490	4038.151
7	567	454	4718.006
8	526	422	5399.814
9	491	389	6083.574
10	454	360	6769.287
11	420	331	7456.952
12	386	304	8146.568
13	359	278	8838.135
14	330	254	9531.651
15	301	232	10 227.115
16	275	209	10 924.526
17	249	187	11 623.882
18	227	169	12 325.181
19	205	150	13 028.421
20	184	135	13 733.600
21	165	120	14 440.714
22	147	104	15 149.761
23	132	92	15 860.737
24	115	79	16 573.639
25	102	68	17 288.463
26	89	59	18 005.203
27	76	51	18 723.856
28	65	41	19 444.415
29	55	35	20 166.876
30	47	28	20 891.231
31	38	23	21 617.475
32	31	18	22 345.600
33	26	14	23 075.600
34	20	10	23 807.467
35	16	7	24 541.193
36	11	5	25 276.770
37	9	3	26 014.188
38	6	2	26 753.440
39	4	1	27 494.517
39 40	3	0	28 237.409
40 41	3 1	0	28 982.106
41	1	0	29 728.599

41, 42, respectively. Clearly, there is no need to include  $v^{(K)}$ functions when K > 42 and we therefore set  $K_{\text{max}}$  is 42. The lowest level for each K is labelled by  $v_2 = K$ ,  $l_2 = K$ . The fundamental bend frequency is 668 cm<sup>-1</sup>. At K = 42, only the lowest state with energy 29 729 cm<sup>-1</sup> is included see Table 4.

We can directly compare our N with those of Zak et al.<sup>24</sup> because we use the same coordinates and KEO and compute the same  $v^{(K)}$ . We use an ALF basis and they use a DVR basis, but this should not affect the required number of  $v^{(K)}$ . Since our J = 100 levels are well converged, we can be certain that there is no need to use N = 100 functions for K > 42 (we use zero). Moreover, using N = 100 functions for  $0 \le K \le 41$  is probably inadequate for small K. We have N = 885 for K = 0. Even though our final basis size is similar to theirs for computing I = 100levels (they have 10100 functions and we have 10134), we expect that our basis functions are better and our levels are better converged.

Table 5 Comparison between our A+ symmetry levels and Huang2022 levels for select J.  $\varDelta_{\rm 15k}/\varDelta_{\rm 20k}$  are the maxium absolute differences between our levels and Huang2022 levels up to 15 000/20 000 cm<sup>-1</sup>, respectively. Our levels are obtained from two-step calculations with  $E_{cut} = 30000$ cm $^{-1}$ . A complete list of energy levels up to J = 100 is available from the authors

	$N_{ m bas}$	$N_{ m level}$	$\Delta_{15\mathrm{k}}$	$\Delta_{20\mathrm{k}}$
J = 10(even)	6605	1780	0.00184	0.00203
J = 20(even)	9185	2151	0.00210	0.01966
J = 30(even)	10014	2102	0.00207	0.05755
J = 40(even)	10 133	1998	0.00205	0.10287
J = 50(even)	10 134	1871	0.00205	0.04117
J = 60(even)	10 134	1724	0.00201	0.02665
J = 70(even)	10 134	1557	0.00182	0.02060
J = 74(even)	10 134	1487	0.00181	0.01067
J = 80(even)	10 134	1388	0.00180	0.00713
J = 90(even)	10 134	1207	0.00150	0.00299
J = 100(even)	10 134	1036	0.00147	0.00204
J = 11(even)	6051	1554	0.00013	0.00152
J = 31(even)	9152	1822	0.00012	0.02617
J = 75(even)	9249	1260	0.00013	0.00581

Although in our final calculations, we use only  $|v^{(K)}\rangle$ ,  $K \leq 42$ , we actually compute  $|v^{(K)}\rangle$  for higher *K* because they can be used to converge levels higher than those we publish in this paper. A good general rule of thumb is to choose  $N_{\theta}$  (the number of Gauss Legendre quadrature points) to be at least one larger than the highest degree of the ALF basis. So we use  $N_{\theta} = K + l_x + 1$ . When  $K \leq 50$ , we use  $N_{\theta} = 201$ , regardless of K. For smaller values of K, we have more points than we need, but it is advantageous to evaluate the potential at a single set of points for all  $K \leq 50$ . When  $100 \ge K > 50$ , we use  $N_{\theta} = 251$ .

It is interesting to compare our basis sizes with the basis sizes in the calculation of Schwenke and co-workers. Take the J = 100 A + calculation as an example with data from ref. 46. They use a series of intermediate contracted functions. To compute 1-D contracted bend functions for each K, up to K = 100, they use a large threshold at 0.6 Hartree (132 000 cm<sup>-1</sup>). A large threshold is required because in their scheme stretch-bend coupling is incorporated only at the end. They use 1371 bendrotation eigenfunctions with energies less than 0.26 Hartree

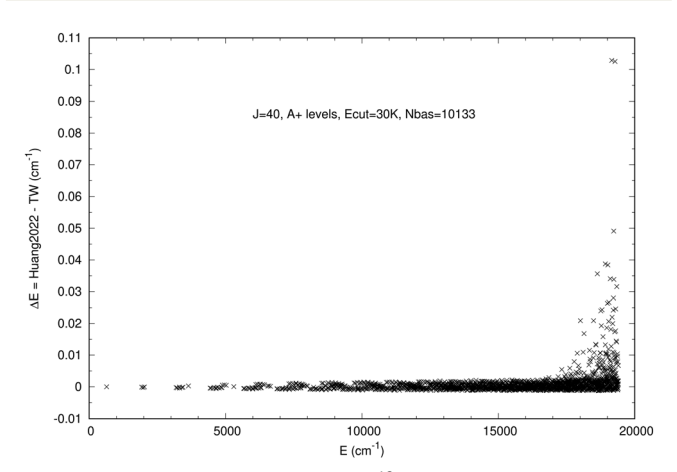


Fig. 2 Differences between Huang2022<sup>46</sup> and our levels (TW) for J = 40A+ levels computed with  $E_{\text{cut}} = 30\,000 \text{ cm}^{-1}$ 

Paper

Table 6 Comparison between our levels and Huang2022 levels for a select window of J = 40 A+ levels. Shown are the 1704th state to 1748th state.  $\Delta_{22}$  = Huang2022 - TW.  $\Delta_{17}$  = Huang2017 - TW. TW is this work. Our levels are obtained from two-step calculations obtained with  $E_{cut}$  = 30 000  $\,\mathrm{cm}^{-1}.$  For our calculation,  $c_1$  and K are the coefficient of the dominant  $v^{(K)}$  state and its K, respectively.  $c_1$  for the Huang calculation is the largest coefficient from their final diagonalization

					TW		Huang202
i	TW	Huang2022	$\varDelta_{22}$	$\Delta_{17}$	$c_1$	K	$c_1$
1704	19 156.7432	19156.8461	0.1029	1.1192	0.984	0	0.338
1705	19 157.7489	19 157.7498	0.0009	0.1299	0.794	10	0.365
1706	19 157.8551	19 157.8552	0.0001	4.1004	0.886	14	0.401
1707	19 162.3062	19 162.3087	0.0025	0.1802	0.785	6	0.303
1708	19 166.7170	19 166.7163	-0.0007	0.0018	0.993	14	0.462
1709	19 170.7940	19 170.8160	0.0220	1.3095	0.806	4	0.249
1710	19 172.7332	19 172.7324	-0.0008	0.1552	0.971	8	0.295
1711	19 173.1855	19 173.1851	-0.0004	0.0106	0.957	14	0.291
1712	19 180.2584	19 180.2630	0.0047	0.3436	0.811	2	0.268
1713	19 186.0207	19 186.0239	0.0032	0.2734	0.903	6	0.282
1714	19 187.1353	19 187.1358	0.0005	0.1136	0.805	9	0.376
1715	19 188.6595	19 188.6603	0.0008	0.0747	0.867	4	0.361
1716	19 192.5329	19 192.5350	0.0022	0.1184	0.791	7	0.429
1717	19 192.5890	19 192.6090	0.0200	1.2873	0.763	3	0.260
1718	19 196.8614	19 196.8604	-0.0010	0.0022	0.994	18	0.353
1719	19 201.7280	19 201.7390	0.0110	0.8847	0.677	5	0.223
1720	19 206.4734	19 206.4784	0.0050	0.2523	0.863	1	0.322
1721	19 212.2731	19 212.2972	0.0242	1.3899	0.532	3	0.209
1722	19 213.5329	19 213.5324	-0.0006	0.1487	0.904	0	0.186
1723	19 214.9835	19 214.9825	-0.0000 $-0.0010$	0.1437	0.904	14	0.391
1723	19 217.7811	19217.7800	-0.0010 $-0.0011$	0.0010	0.996	22	0.391
1724	19217.7811	19217.7800	-0.0011 $0.0017$	0.0010	0.990	11	0.500
						1	
1726 1727	19 220.0152 19 224.8071	19 220.0432	0.0280	1.6477 0.5205	0.673	6	0.177
1728		19 224.8136	0.0064		0.728	2	0.265
	19 228.7026	19 228.7517	0.0491	1.4633	0.935		0.281
1729	19 229.7148	19 229.7182	0.0034	1.7122	0.934	5	0.336
1730	19 231.4000	19 231.4019	0.0019	0.4021	0.965	9	0.480
1731	19 231.9591	19 231.9579	-0.0012	0.0002	0.999	26	0.511
1732	19 232.9690	19 232.9710	0.0020	0.0350	0.980	9	0.312
1733	19 235.5377	19 235.5716	0.0338	1.7576	0.782	0	0.229
1734	19 237.4706	19 237.4699	-0.0007	0.1428	0.895	2	0.218
1735	19 238.2693	19 238.2712	0.0019	0.0152	0.970	15	0.521
1736	19 238.3057	19 238.3165	0.0108	0.9118	0.879	6	0.405
1737	19 242.5116	19 242.5141	0.0025	0.2223	0.923	4	0.298
1738	19 249.1103	19 249.1105	0.0002	0.1479	0.968	8	0.510
1739	19 252.0979	19 252.1000	0.0021	0.0074	0.986	19	0.542
1740	19 255.9739	19 255.9771	0.0032	0.2162	0.846	2	0.372
1741	19 258.6060	19 258.6083	0.0023	0.0033	0.995	23	0.639
1742	19 258.6561	19 258.6661	0.0099	0.8936	0.787	0	0.277
1743	19261.5275	19261.5360	0.0084	0.5474	0.533	0	0.276
1744	19 263.8262	19263.8260	-0.0002	0.0224	0.964	8	0.377
1745	19 266.2800	19266.2817	0.0017	0.0648	0.938	1	0.280
1746	19 266.7688	19266.7862	0.0174	1.3271	0.654	3	0.236
1747	19274.1744	19274.1775	0.0032	0.2293	0.844	2	0.268
1748	19 277.6829	19 277.7854	0.1025	3.8847	0.963	0	0.247

 $(57\,000\,\mathrm{cm}^{-1})$  (not 0.15 Hartree stated in their paper<sup>27</sup>). The 1371 bend-rotation functions are then coupled to stretch functions to make a final basis with 147 671 functions using a threshold of 0.3 Hartree (66 000 cm<sup>-1</sup>). Because they use a direct eigensolver, there are unable to calculate eigenvalues in a basis this large and they therefore truncate it keeping only 45 000 functions. We also use a direct eigensolver for the final diagonalization, but our final basis size has only about 10 000 basis functions and is determined with a single low threshold of  $E_{\rm cut}$  = 30 000 cm<sup>-1</sup>. See Fig. 2 and Table 6, for a comparison of our levels with those of Huang et al. for J = 40.

### IX. Conclusion

In this paper, we propose a two-step method that uses an associated Legendre function basis and a K-independent quadrature. The advantage of the two-step idea is that the largest rovibrational term in the KEO does not have off-diagonal matrix elements in the  $|v^{(K)}\rangle|JKM\rangle$  basis. It is common to compute the  $|v^{(K)}\rangle$  functions in a basis of K-dependent DVR functions. A DVR seems appealing because the potential matrix in a DVR is diagonal. However, when using a K-dependent DVR, matrix elements of coordinate dependent factors in the KEO must be transformed from the ALF basis to the DVR. This is more complicated and more costly than using the ALF basis directly. If the ALF basis is used directly then these transformations are not necessary. However, when the ALF basis is used, it is necessary to either compute matrix-vector products with or calculate matrix elements of the potential. Fortunately, this is easily done, using a single set of (K-independent) quadrature points for all K, by evaluating sums sequentially.  $^{17,53-55}$  When one uses the ALF basis and quadrature (i.e. a finite basis representation<sup>17</sup>) rather than the corresponding DVR, one must transform the potential instead of the kinetic matrix. Whereas, transforming the kinetic matrix is complicated by the fact that the DVR is K-dependent, there is no need to use K-dependent points and weights when doing potential matrix elements by quadrature. Using a K-dependent DVR also requires evaluating the potential at different sets of points for each K. Another difference between our two-step method and the most popular two-step code<sup>5,6</sup> is that we compute the  $|\nu^{(K)}\rangle$  with a Lanczos eigensolver. This makes it possible to use a large primitive basis whose functions are products of 1-D functions. The alternative is to use a sequence of contractions which works well, but requires additional steps. Iterative methods become essential for larger molecules, but are also useful for triatomics.

The two-step method was first used for H<sub>2</sub>D, but it is most advantageous for linear molecules because the ro-vibrational coupling term incorporated into the Hamiltonian whose eigenfunctions are the  $|v^{(K)}\rangle$  basis functions is much larger for linear molecules. When it is large, the energies that correspond to  $|v^{(K)}\rangle$  increase rapidly with K (when K is increased to K + 1 the energy of the lowest  $|v^{(K)}\rangle$  increases by about the bend frequency). Because  $|v^{(K)}\rangle$  with large energies are less important, the number of  $|v^{(K)}\rangle$  which must be used to compute final energies and wavefunctions, below a chosen threshold, decreases with K. That number is actually zero if K is large enough. In some previous two-step calculations the number of  $|v^{(K)}\rangle$  has been chosen to be independent of K.

An efficient method for computing ro-vibrational levels of a linear triatomic molecule will also be useful for studying van der Waals complexes for which at least one of the constituents is a linear molecule. This is because a good basis is composed of products of intra- and inter-molecular functions. 56,57

#### Conflicts of interest

There are no conflicts to declare.

## Acknowledgements

This work has been supported by the Natural Sciences and Engineering Research Council of Canada and the Digital Alliance of Canada. TC thanks the Jean d'Alembert fellowship program for its support at the Université Paris-Saclay. XGW thanks Donghui Zhang's group at the Dalian Institute of Chemical Physics for hospitality. We thank Xinchuan Huang and David Schwenke and Emil Zak for detailed and helpful discussions.

#### References

- 1 G. D. Carney, L. L. Sprandel and C. W. Kern, Adv. Chem. Phys., 1978, 37, 305.
- 2 J. Tennyson, Comput. Phys. Rep., 1986, 4, 1.
- 3 S. Carter and N. C. Handy, Comput. Phys. Commun., 1988, 51, 49.
- 4 P. Jensen, J. Mol. Spectrosc., 1988, 128, 478.
- 5 J. Tennyson, J. R. Henderson and N. G. Fulton, Comput. Phys. Commun., 1995, 86, 175.
- 6 J. Tennyson, M. A. Kostin, P. Barletta, G. J. Harris, O. L. Polyansky, J. Ramanlal and N. F. Zobov, Comput. Phys. Commun., 2004, 163, 85-116.
- 7 D. W. Schwenke, J. Chem. Phys., 2015, 142, 144107.
- 8 M. J. Bramley and N. C. Handy, J. Chem. Phys., 1993, 98, 1378-1397.
- 9 J. Tennyson and B. T. Sutcliffe, Mol. Phys., 1986, 58, 1067.
- 10 T. Carrington, J. Chem. Phys., 2017, 146, 120902.
- 11 P. Sarkar, N. M. Poulin and T. Carrington, J. Chem. Phys., 1999, **110**, 10269.
- 12 Z. Bačić and J. C. Light, Annu. Rev. Phys. Chem., 1989, 40, 469.
- 13 M. Mladenovic, Spectrochim. Acta, Part A, 2002, 58, 809.
- 14 F. T. Smith, Phys. Rev., 1960, 120, 1058.
- 15 B. R. Johnson and W. P. Reinhardt, J. Chem. Phys., 1986, **85**, 4538.
- 16 J. C. Light, I. P. Hamilton and J. V. Lill, J. Chem. Phys., 1985, **82**(3), 1400–1409.
- 17 J. C. Light and T. Carrington Jr., Adv. Chem. Phys., 2000, 114, 263-310.
- 18 J. M. Bowman, T. Carrington and H.-D. Meyer, Mol. Phys., 2008, 106, 2145-2182.
- 19 H. Massol, et al., Space Sci. Rev., 2016, 205, 153.
- 20 M. Snels, S. Stefani, D. Grassi, G. Piccioni and A. Adriani, Planet. Space Sci., 2014, 103, 347.
- 21 I. E. Gordon, et al., J. Quant. Spectrosc. Radiat. Transfer, 2017,
- 22 B. Connor, et al., Atmos. Meas. Tech., 2016, 9, 5227.
- 23 F. Oyafuso, et al., J. Quant. Spectrosc. Radiat. Transfer, 2017, 203, 213.
- 24 E. J. Zak, J. Tennyson, O. L. Polyansky, L. Lodi, S. A. Tashkun and V. I. Perevalov, J. Quant. Spectrosc. Radiat. Transfer, 2016, 177, 31.
- 25 X. Huang, D. W. Schwenke, S. A. Tashkun and T. J. Lee, J. Chem. Phys., 2012, 136, 124311.

- 26 X. Huang, D. W. Schwenke, R. S. Freedman and T. J. Lee, J. Quant. Spectrosc. Radiat. Transfer, 2017, 203, 224.
- 27 X. Huang, D. W. Schwenke, R. S. Freedman and T. J. Lee, J. Phys. Chem. A, 2022, 126, 5940.
- 28 S. N. Yurchenko, T. M. Mellor, R. S. Freedman and J. Tennyson, Mon. Not. R. Astron. Soc., 2020, 496, 5282–5291.
- 29 S. Carter, N. C. Handy and B. T. Sutcliffe, Mol. Phys., 1983, 49, 745.
- 30 X.-G. Wang and T. Carrington, Jr., J. Chem. Phys., 2017, 146, 104105.
- 31 J. Tennyson and B. Sutcliffe, Int. J. Quantum Chem., 1992, 42, 941-952.
- 32 S. Carter and N. C. Handy, J. Chem. Phys., 1987, 87, 4294.
- 33 S. Carter, N. C. Handy and I. M. Mills, Philos. Trans. R. Soc. London, Ser. A, 1990, 332, 309.
- 34 G. Yan, D. Xie and A. Tian, J. Phys. Chem., 1994, 98, 8870-8875.
- 35 H. Partridge and D. W. Schwenke, J. Chem. Phys., 1997, 106, 4618.
- 36 J. Zúñiga, A. Bastida, M. Alacid and A. Requena, J. Mol. Spectrosc., 2001, 205, 62.
- 37 J. Cerezo, A. Bastida, A. Requena and J. Zúñiga, J. Quant. Spectrosc. Radiat. Transfer, 2014, 147, 233.
- 38 X.-G. Wang and T. Carrington Jr, Mol. Phys., 2012, 110(9-10), 825-835.
- 39 X.-G. Wang and T. Carrington, Jr., J. Chem. Phys., 2013, 138, 104106.
- 40 D. W. Schwenke and D. G. Truhlar, Comput. Phys. Commun., 1984, 34, 57.
- 41 S. Carter and N. C. Handy, Mol. Phys., 1986, 57, 175.
- 42 A. A. A. Azzam, J. Tennyson, S. N. Yurchenko and O. V. Naumenko, Mon. Not. R. Astron. Soc., 2016, 460, 4063-4074.
- 43 D. W. Schwenke, J. Phys. Chem., 1996, 100, 2867.
- 44 P. R. Bunker and J. M. R. Stone, J. Mol. Spectrosc., 1972, 41, 310-332.
- 45 X.-G. Wang and T. Carrington Jr., J. Chem. Phys., 2004, 121, 2937.
- 46 X. Huang, private communication, November, 2023.
- 47 S. N. Yurchenko and T. M. Mellor, J. Chem. Phys., 2020, 153, 154106.
- 48 X. G. Wang and T. Carrington, RV3: A package of programs to compute rovi-brational levels and wavefunctions of triatomic molecules.
- 49 H. Wei and T. Carrington Jr., J. Chem. Phys., 1992, 97, 3029.
- 50 J. Tennyson and B. T. Sutcliffe, J. Chem. Phys., 1982, 77, 406.
- 51 X.-G. Wang and T. Carrington, Jr., J. Chem. Phys., 2015, 143, 024303.
- 52 ESI† for J = 0 A+ levels up to 20 000 cm<sup>-1</sup>, and all the levels referred to in Table 5.
- 53 M. J. Bramley and T. Carrington, Jr., J. Chem. Phys., 1993, 99, 8519.
- 54 U. Manthe and H. Köppel, J. Chem. Phys., 199093, 345.
- 55 X.-G. Wang and T. Carrington, Jr., J. Chem. Phys., 2014, 141, 154106.
- 56 P. M. Felker and Z. Bačić, J. Chem. Phys., 2019, 151, 024305.
- 57 X.-G. Wang and T. Carrington, Jr., J. Chem. Phys., 2018, 148, 074108.